Supporting Information

All-graphene-contact electrically pumped on-demand transferrable nanowire source

*Min-Woo Kim†, Sun-Wook Park†, Kyong-Tae Park†, Byung-Ju Min†, Ja-Hyun Ku, Jin-Yong Ko, Jin Sik Choi and You-Shin No**

Department of Physics, Konkuk University, Seoul 05029, Republic of Korea

This file includes:

Methods

Supporting Information Figures S1–S10

References

Methods

Fabrication of nanowires. A 3-inch epitaxially grown AlGaInP/GaAs LED wafer (Optowell Co., Ltd., RED LED epi-wafer) with a multi-quantum well (MQW) structure was used to fabricate an array of nanowires (NWs) (Supplementary Figure 1a for the detailed wafer structure). After a brief surface cleaning, the wafer was spin-coated with a few-hundred-nanometer-thick polymethylmethacrylate (PMMA, MicroChem, PMMA C4) resist. Electron-beam lithography (EBL) was then carried out to generate the cross-linked negative polymer patterns for the arrays of nanoscale wires and the bulk supporting mesa structures. Following 2-min development with acetone, the wafer was subjected to a 30-sec chemically assisted ion-beam etching (CAIBE) process at room temperature; this process allowed wide exposure of the AlAs sacrificial layer to air. To prevent fast oxidation of the AlAs layer, the wafer was quickly submerged in a buffered oxide etchant (BOE, J.T. Baker, 40% NH_4F:49% HF = 10:1) for 2-min at room temperature; the AlAs underneath the wires (the mesa structures) was also completely (partially) wet-etched. Lastly, the application of a 20-min O_2-plasma reactive ion-etching (RIE) removed the residual resist on top of the sample, yielding an array of air-suspended NWs and bulk mesa structures that supported the NWs.

Fabrication of Si_3N_4 strip-type photonic waveguides. An array of strip-type photonic waveguides (SPWGs) was fabricated by using a low-pressure chemical vapor deposition (LPCVD)-grown 200-nm-thick Si_3N_4 / 500-nm-thick SiO_2 wafer. EBL was applied using a positive polymer resist (EM Resist, Ltd., SML600) to generate the SPWG array pattern. The RIE process was used to vertically etch the sample and define the waveguide (WG) patterns. An additional 20-min O_2-plasma cleaning removed the residual resist and completed the fabrication process.

Synthesis of multilayer graphene. Multilayered graphene (MLG) was synthesized via chemical vapor deposition (CVD) by using a 300-nm-thick Ni metal thin-film catalyst. The Ni/SiO_2 substrate was prepared by depositing Ni onto a thermally oxidized Si wafer. The quartz substrate-supported Ni substrate was heated to 1000 °C inside the tube-type CVD chamber. A mixture of methane and hydrogen gas (CH_4:H_2 = 5:10) was flowed through the chamber for 40-min. Following thermal annealing application[1], the gas mixture was substituted with an inert gas (Ar), and then rapidly cooled by moving the heater from the growing zone to the cooling zone.

Multilayer graphene wet-transfer. Before the transfer, the target chip was dipped in an acetone solution and ultrasonicated for 2-min. and rinsed with isopropyl alcohol (IPA) and deionized (DI) water several times. Following MLG growth, the PMMA C4 was coated on the MLG-grown substrate at 4500 rpm for 45-sec by using a spin coater. To separate the PMMA/MLG structure from the SiO_2 substrate, the MLG-grown substrate was floated overnight on a Cu-etchant consisting of 0.5 M $FeCl_3$. After rinsing the structure several times with DI water, we transferred the PMMA/MLG structure onto a clean spare substrate and maintained it for a few minutes. Before the DI water was completely dried out, we dipped the chip in a solution of DI water and re-floated the PMMA/MLG. Then we finally transferred the PMMA/MLG onto target chip. When the DI water was dried out, the PMMA/MLG/substrate was annealed for 30-min by using a hot plate at 180 °C under ambient conditions. The PMMA was removed by applying acetone and rinsed by applying IPA. This removal/cleaning process was carried out before lithographic patterning step to make sure the clean interfaces between the graphene and NW. In addition, PMMA residue on top surface of NW was completely removed during the O_2-plasma process. Lastly, we performed

high-vacuum annealing (base pressure: < 10^{-7} Torr) at 350 °C for 3-hour to remove all PMMA residue.

Electroluminescence measurement. A fully fabricated device chip was firmly mounted on a mechanically stable XYZ stage with a nanoscale translation step (Newport, M-562-XYZ) after the thermal annealing process was applied to reduce the graphene/metal contact resistance. An additional rotational stage was also used, when necessary (e.g., for angle-resolved spectroscopic measurement), to change the angular position of the device. Continuous-wave (CW) or pulsed-wave (1 ms pulse width and 30% duty cycle) currents were injected into the NW device through the two tungsten probe tips that were connected to a semiconductor parameter analyzer (Keithley, 4200-SCS) or a function generator (Tektronix, AFG3011C). Pulsed-wave operation was used only for angle-resolved electroluminescence (EL) measurements. The semiconductor analyzer simultaneously recorded the applied voltages, read the currents passing through the device, and yielded the current-voltage characteristic curve. A ×50 microscope objective lens with a numerical aperture of 0.42 (Mitutoyo, M Plan Apo ×50) was used to collect the light emitted from the device and transmit it to either a charge-coupled device (CCD) camera (QImaging, optiMOS™ Scientific CMOS Camera) for EL imaging or a spectrometer (Princeton Instruments, Acton SpectraPro SP-2300) including an array detector (Princeton Instruments, PIXIS100B) for spectroscopy. A tungsten halogen lamp (Thorlabs, OSL2) was used as the illumination source. To obtain the angle-resolved measurement, a linear polarizer (Thorlabs, WP25M-VIS) was installed in front of the CCD camera or spectrometer.

Numerical simulations. We employed a finite-difference time-domain method (Lumerical, FDTD solutions) to calculate the relative light absorption of graphene and metal contacts, and the modal dispersions, the electric field and intensity profiles, and the electric dipole powers and transmitted powers along the SPWG. In relative light absorption simulation, we employed single NW device structure used in experiment (Figure 3c), including a 9-μm-long AlGaInP NW and graphene contacts and various metal contacts. The perfectly matched layers were applied at the boundary of the calculation domain with dimensions of 13 μm × 4 μm × 4 μm. The refractive index of AlGaInP was set to 3.49. For graphene and various metals (e.g., Ti, Al, Pd, Ni, Cr, Au), we used optical constants from the references[2-4]. For the dispersions, we applied the two-dimensional finite-difference eigenmode (Lumerical, MODE solutions) to calculate the wavenumbers, eigenfrequencies, and field profiles of the guided modes. An infinitely long single strip Si_3N_4 WG with a respective width and thickness of 730 and 200 nm was placed on a SiO_2 substrate. Perfectly matched layers were applied at the boundary of the calculation domain with dimensions of 2 μm × 1 μm. In the three-dimensional waveguide simulation, a 6-μm-long AlGaInP NW with a width and thickness of 730 and 200 nm was placed at the center of the coupling region of the Si_3N_4 SPWG. Regarding the other materials (e.g., Si_3N_4, SiO_2, and Si), we applied optical constants from the widely used references[4, 5]. The perfectly matched layers were applied at the boundary of the calculation domain with dimensions of 100 μm × 14 μm × 8 μm. Electric dipoles with different polarizations were generated at the center of the NW to simulate the light emission, coupling, and waveguiding.

Supporting Information Figures

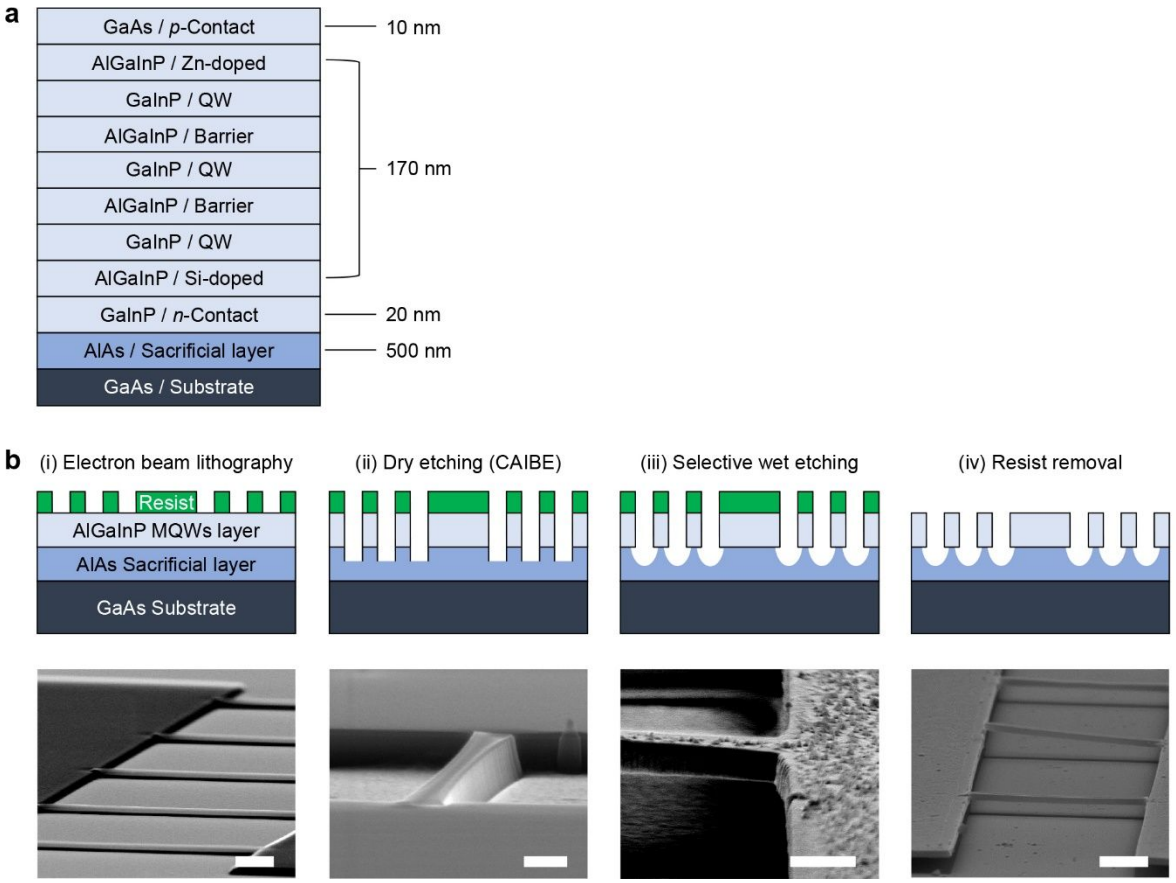

Figure S1. Structure of LED wafer and NWs fabrication process. (a) Schematic showing the detailed compositional and electrical structures of the wafer. It consists of a 10-nm-thick *p*-GaAs (contact), 170-nm-thick AlGaInP/GaInP 3QWs, 20-nm-thick *n*-GaInP (contact), and 500-nm-thick AlAs sacrificial layers with a GaAs substrate. (b) Schematics (top) and scanning electron microscopy (SEM) images (bottom) of the key fabrication steps. (i) A cross-linked PMMA C4 was used to form the negative patterns of the nanoscale wires and bulk rectangular mesa structures through the application of high dosage EBL. Scale bar: 1 μm. (ii) The sample was vertically dry-etched by applying a CAIBE process until the AlAs sacrificial layer was exposed to air. Scale bar:

500 nm. (iii) The AlAs layer underneath the wires (mesa structures) was completely (partially) removed by the selective wet-etching using BOE at room temperature. Scale bar: 500 nm. (iv) The residue of the PMMA mask on top of the AlGaInP slab was removed by applying a 20-min O_2-plasma process. Scale bar: 2 μm.

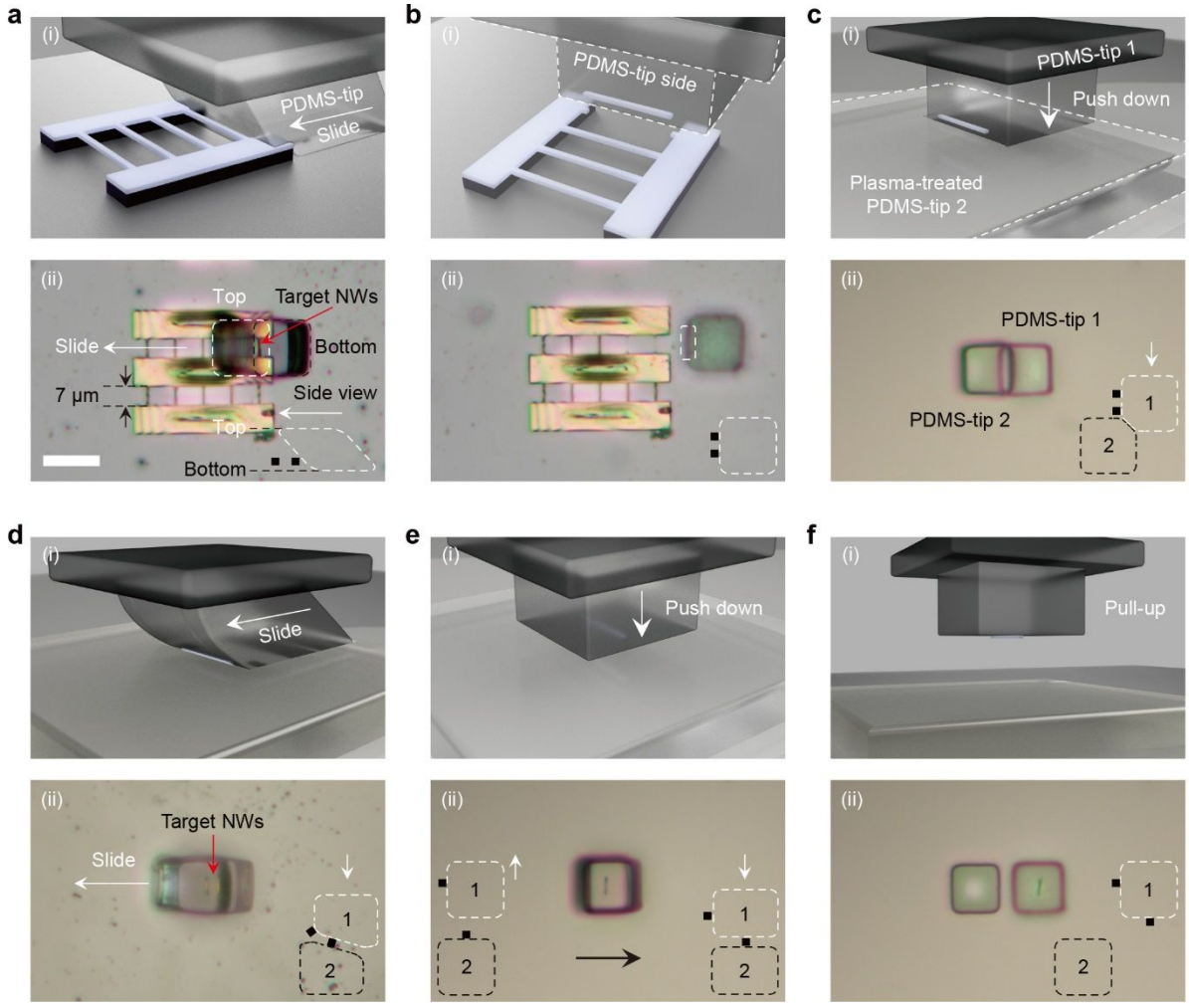

Figure S2. Two-step pick-up and transfer process using two polydimethylsiloxane (PDMS) microtips. (a)–(f) Schematics (top, (i)) and optical microscopy images (bottom, (ii)) illustrating the key steps. The optical image insets show the side views of the PDMS tips (dotted lines) and target NWs (black squares). White arrows mark the direction of movement or applied force. (a) Lateral approach of a microtip (Tip-1) toward a target NW for the first pick up. Bottom of the Tip-1 (black dotted line) was aligned and anchored to the substrate near the target NWs (red arrow). The PDMS tip is flexible enough to be slowly slid in a lateral direction by translating the sample or PDMS-tip stage. Observation of the NWs through the transparent PDMS confirmed that the side of Tip-1 applies mechanical pressure to break the NW terminals. (b) Process of lifting off Tip-1 under the

condition of the target NW being broken and attached to the side of Tip-1. (c)–(d) Tip-to-tip migration of the target NW. Tip-1 was vertically loaded and pressed downward on a part of another surface-treated and upside-down PDMS tip (Tip-2). Contact-sliding Tip-1 in a lateral direction resulted in the NW becoming detached from the side of Tip-1 due to the expansion of contact surface and migrated to the Tip-2. (e)–(f) The second pick-up process. Releasing the contact between the tips and re-aligning Tip-1 to pick up the NW on Tip-2. The NW was more likely attached to the Tip-1 because the plasma treatment decreased the surface adhesion of Tip-2. Scale bar: 20 μm.

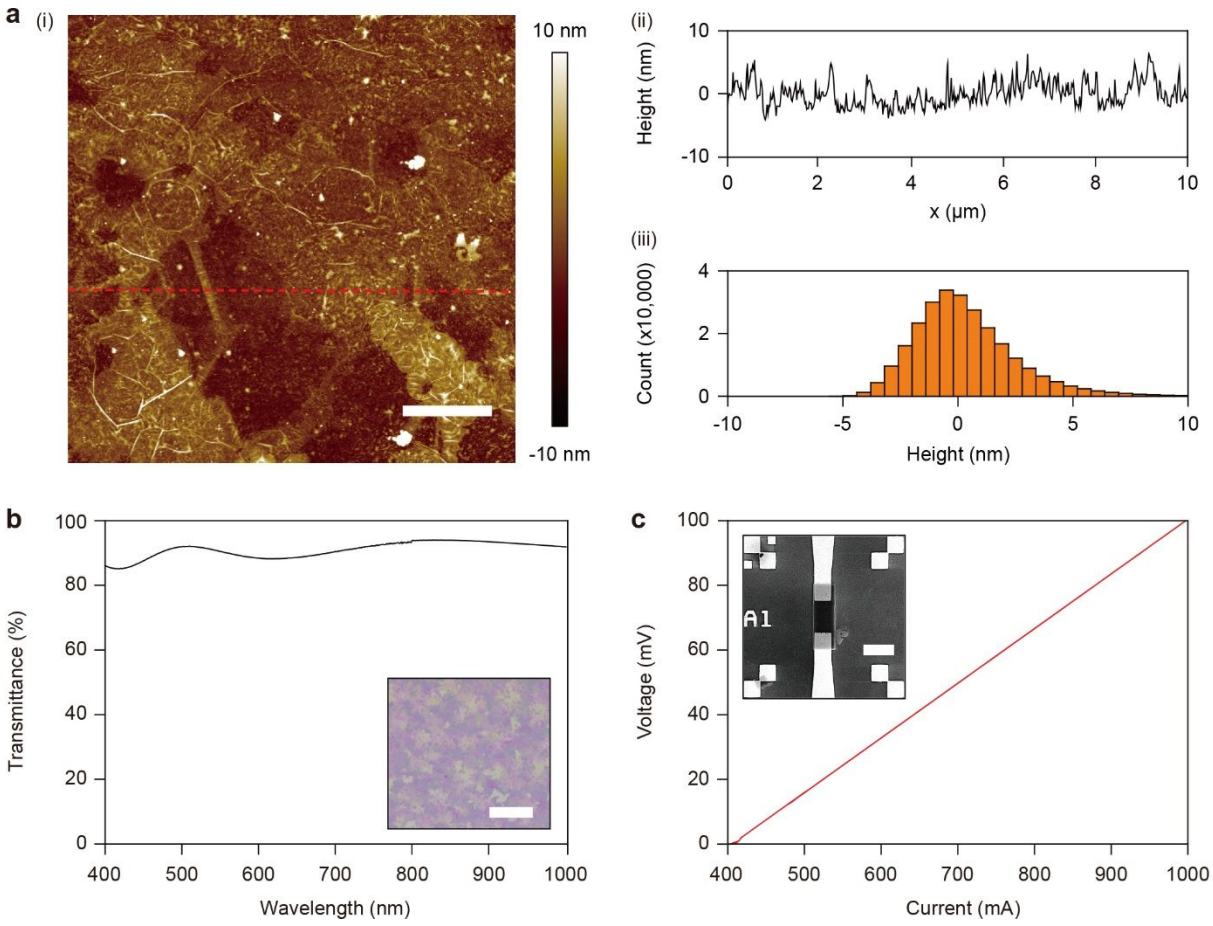

Figure S3. Topographical, optical, and electrical characterization of MLG used in this study. (a) Atomic force microscopy data showing the surface topography of our CVD-grown MLG. (i) Two-dimensional (2D) mapping of height over an area of 10 μm × 10 μm (left). Scale bar: 2 μm. (ii) Line profile of the height following the red dotted line in (i). (iii) Height histogram over the entire 2D map of (i). The measured RMS roughness was ~2.62 nm, which reveals a good uniformity in thickness of our MLG. (b) Measured transmittance spectrum of the MLG sheet. The MLG exhibited high transmittance (i.e., >80%) over a wide range of visible and near-infrared frequencies. Inset: optical microscopy image of the MLG sheet. Scale bar: 20 μm. (c) Measured current-voltage (*I-V*) curve for the MLG channel device with dimensions of 7 μm × 21 μm. The

cross-linked PMMA cover was also applied to the top of the graphene channel to consider the experimental situation in our NW device. Inset: SEM image of the device used for the measurement. Scale bar: 10 μm.

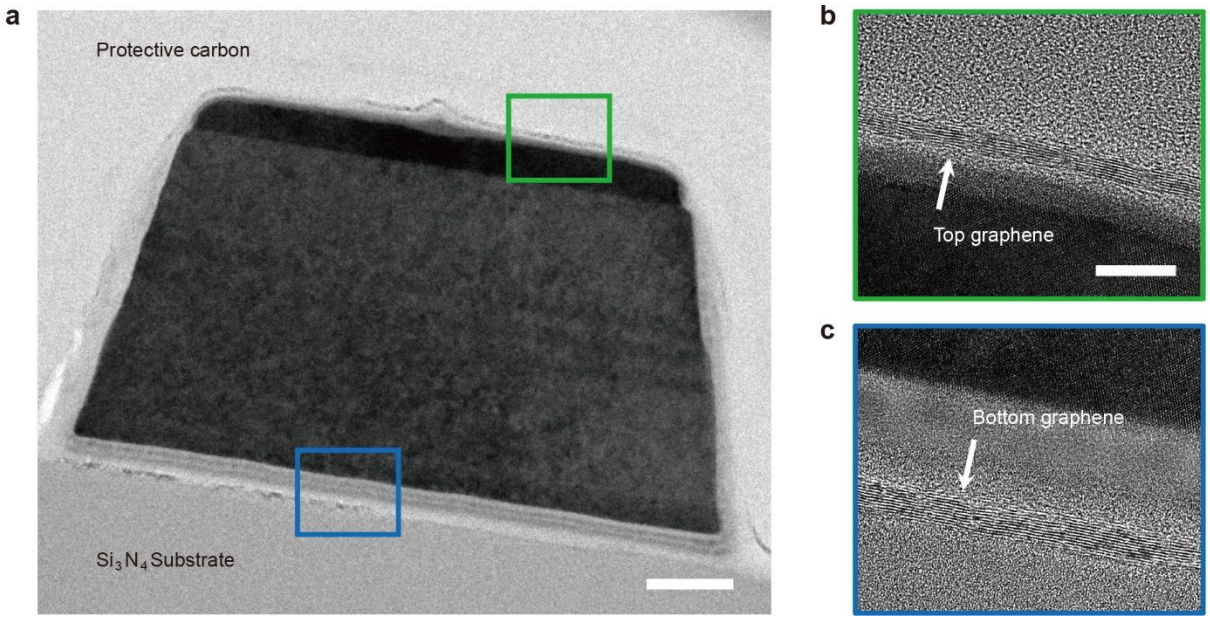

Figure S4. Cross-sectional transmission electron microscopy (TEM) image of the all-graphene-contact NW device. (a) Top (green box) and bottom graphene (blue box) contacts on top of the *n*-type GaAs and bottom of the *p*-type GaInP layers. The MQW structures are visible in the middle. The NW was placed on a Si_3N_4 device substrate. Scale bar: 50 nm. (b)–(c) Magnified TEM images of top (green box in (a)) and bottom graphene contacts (blue box in (a)). Scale bar: 10 nm.

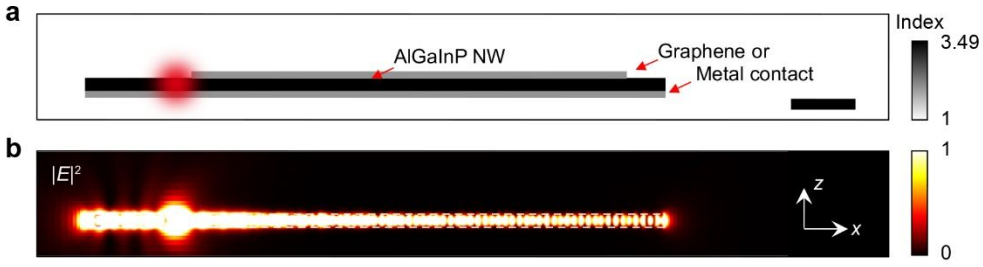

c

Materials	Relative light absorption	Reference
10 layers graphene	1	
Ti 50 nm / Al 150 nm	1.64	[6]
Ti 4 nm / Pd 350 nm	1.61	[7]
Ti 40 nm / Au 200 nm	1.6	[8]
Top: Ni 150 nm / Au 50 nm Bottom: Ti 20 nm / Al 100 nm / Ti 30 nm / Au 50 nm	1.63	[9]
Cr 5 nm / Au 400 nm	1.58	[10]
Pd 40 nm / Ti 10 nm / Au 240 nm	1.57	[11]

Figure S5. Relative light absorption of graphene and various metal contacts. (a) Side view of the simulated structure: AlGaInP NW (black) with graphene or metal contacts (gray). The device structure from the experiment (Figure 3c) was used in this simulation. The dipole sources with different polarizations were introduced at a position where the light emission was observed in experiment (graded red spot). Scale bar: 1 μm. (b) Calculated electric field intensity profile with top and bottom graphene contacts. (c) Relative light absorption in graphene and various metal contacts. Here, the contact structures were all identical, but the thicknesses were adopted from the references in the table. The relative light absorption values of the metals were normalized with the one of graphene. To calculate relative light absorption, we calculated total powers of the dipole sources as P_{dipole} and the powers passing through the imaginary box that contains the NW and the graphene or metal contacts as P_{NW}. Then, the light absorption of the given contact materials can be obtained as follows: $A_{tot} = \sum_{i=x,y,z}(P_{dipole,i} - P_{NW,i})/\sum_{i=x,y,z}P_{dipole,i}$.

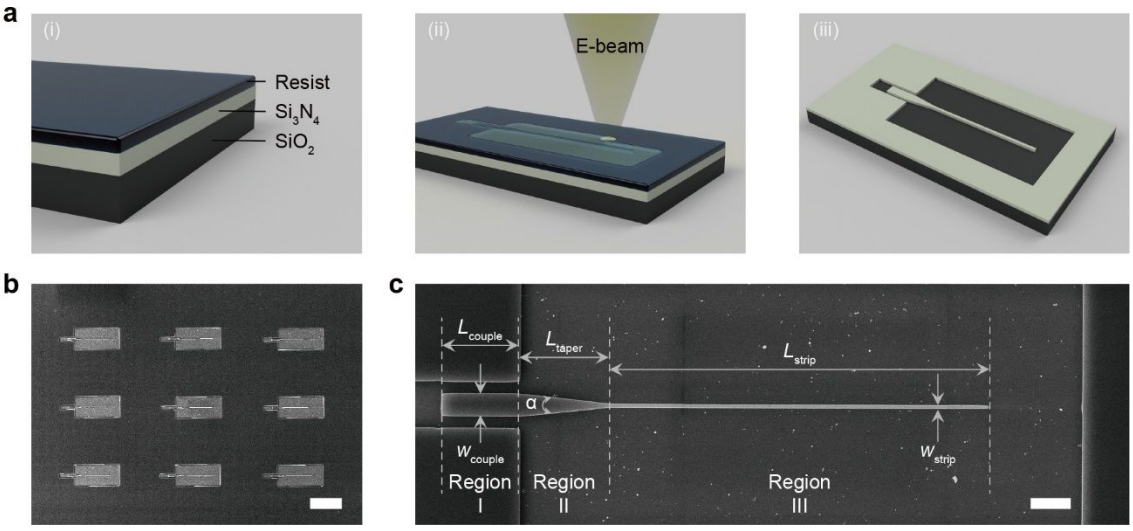

Figure S6. Fabrication process for an array of Si_3N_4 SPWGs. (a) Schematic representations of the fabrication steps. (i) Resist-coating on a LPCVD-grown Si_3N_4/SiO_2 substrate. (ii) EBL or photolithography mask patterning process for an array of SPWGs. (iii) RIE vertical etching. (b)–(c) Low- and high-magnification SEM images of the fabricated SPWGs. (b) A 3 × 3 array of the SPWGs. Scale bar: 50 μm. (c) Image of a single SPWG showing three distinct regions: Region I: region in which a single NW is integrated into the device, Region II: linearly tapered region designed to enable efficient light coupling to the WG modes, and Region III: strip WG region. The lengths of these regions were respectively as follows: L_{couple} = 10 μm, L_{taper} = 11 μm, and L_{strip} = 50 μm. The widths of Regions I and III were w_{couple} = 3 μm, and w_{strip} = 500 nm, respectively. The taper angle was measured to be ~12°. Scale bar: 5 μm.

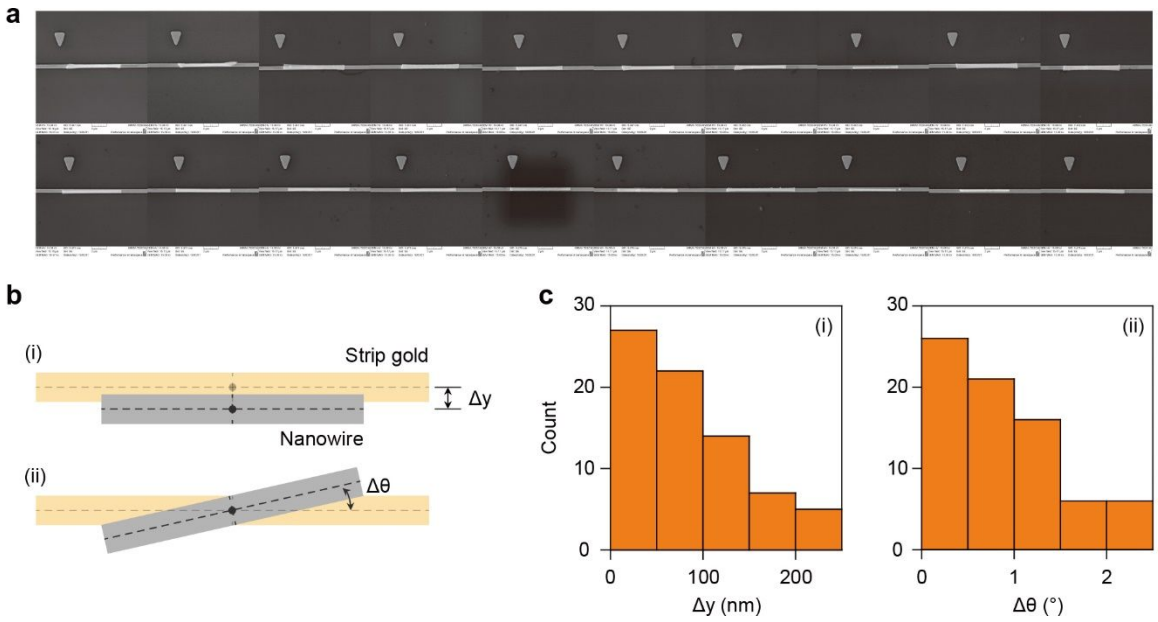

Figure S7. Misalignment measurement of the transferred NW on the single strip WG. (a) Twenty representative SEM images of the transferred NWs on the Au strip WG. The width of the WG was 300 nm. (b) Schematic representations of the translational/vertical (Δy in (i)) and rotational misalignments (Δθ in (ii)). (c) Measured misalignment distribution results for the NWs on the Au strip WGs; (i) translational misalignment, and (ii) rotational misalignment. The total number of transferred NWs implemented in the measurements was 75.

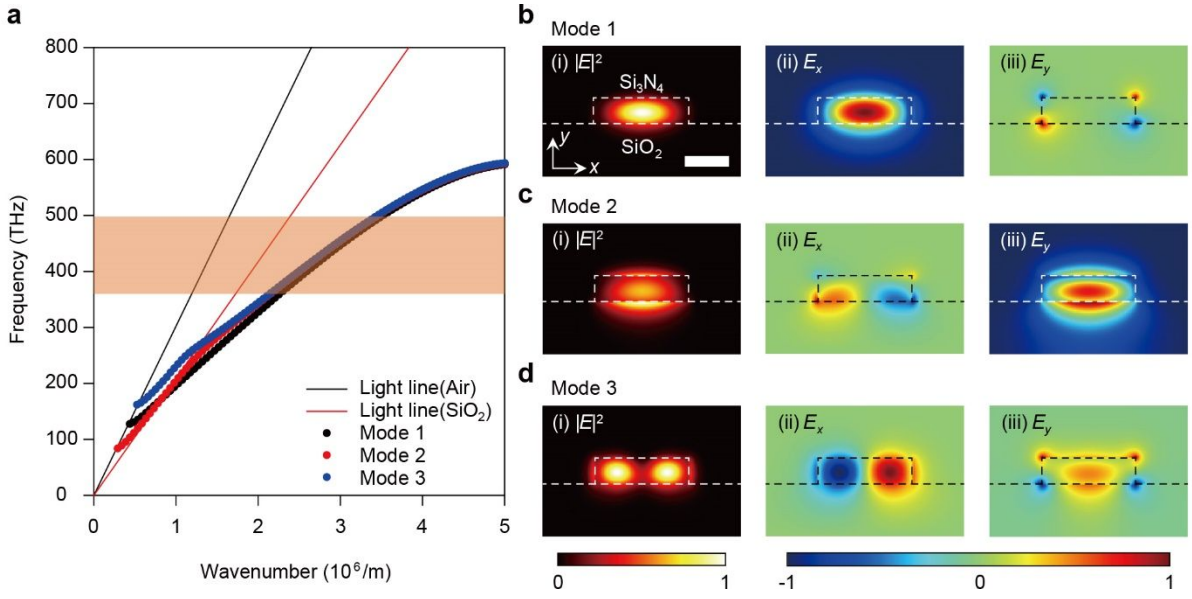

Figure S8. Dispersions and field profiles of the guided modes of a Si_3N_4 strip WG. (a) Dispersion curves for three guided modes: the fundamental transverse-electric-like (TE-like) mode (black dots, Mode 1), fundamental transverse-magnetic-like (TM-like) mode (red dots, Mode 2), and higher-order TE-like mode (blue dots, Mode 3). Note that the light lines through air (black line) and SiO_2 (red line) have been included for references. The orange region denotes the spectral window for the optical gain of the AlGaInP/GaInP MQWs. (b)–(d) Calculated electric field intensities ((i), left), and E_x ((ii), middle) and E_y field profiles ((iii), right) of guided Mode 1 (b), Mode 2 (c), and Mode 3 (d). The intensities and field profiles were collected at a wavelength of 660 nm. White dotted lines indicate the boundaries of the WG and substrate. Scale bar: 200 nm.

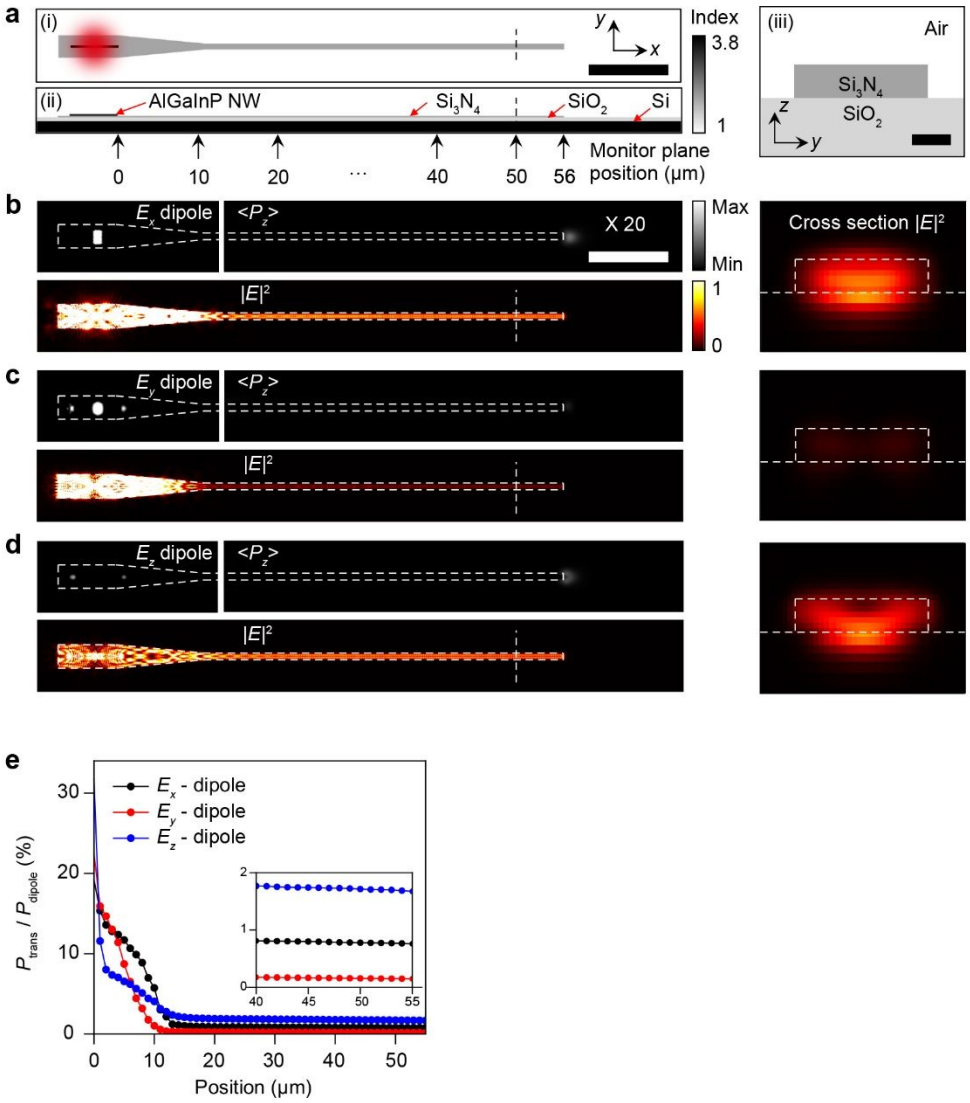

Figure S9. Light emission, coupling, and waveguiding simulation in the SPWG coupled to a single NW light source. (a) Top (*xy* plane, (i)), side (*xz* plane, (ii)), and cross-sectional (*yz* plane, (iii)) views of the following simulated structures: AlGaInP NW (black), Si_3N_4 SPWG (dark gray), and SiO_2 (light gray) and Si substrate. Black arrows along the SPWG mark the positions at which the transmitted powers were monitored. Electric dipoles with different polarizations were generated at the center of the NW (graded red circle, (i)). Scale bars in (i) and (iii) are 10 μm and 100 nm, respectively. (b)–(d) Calculated *z*-components of time-averaged Poynting vectors (top, left), and

electric field intensities (bottom, left). The Poynting vectors were collected at a position 500 nm above the NW; the intensities were collected at the middle of the SPWG. The Poynting vectors and field intensities in (b)–(d) were normalized according to their maximum values. The Poynting vectors at the end of the WG, as shown in (b)–(d), were increased 20-fold to enable direct comparison. NW cross-section field intensity calculations were performed for a position corresponding to 50 μm away from the NW. The generated electric dipoles are denoted as E_x (b), E_y (c), and E_z polarizations (d), respectively. Scale bar: 10 μm. (e) Normalized transmitted powers, P_{trans}/P_{dipole} (i.e., transmission), as a function of the monitoring position along the SPWG. Here, P_{dipole} represents the dipole power at a wavelength of 660 nm. The normalized transmitted powers rapidly decreased in the tapering region and gradually approached a certain value (inset) as the distance from the end of the WG decreased.

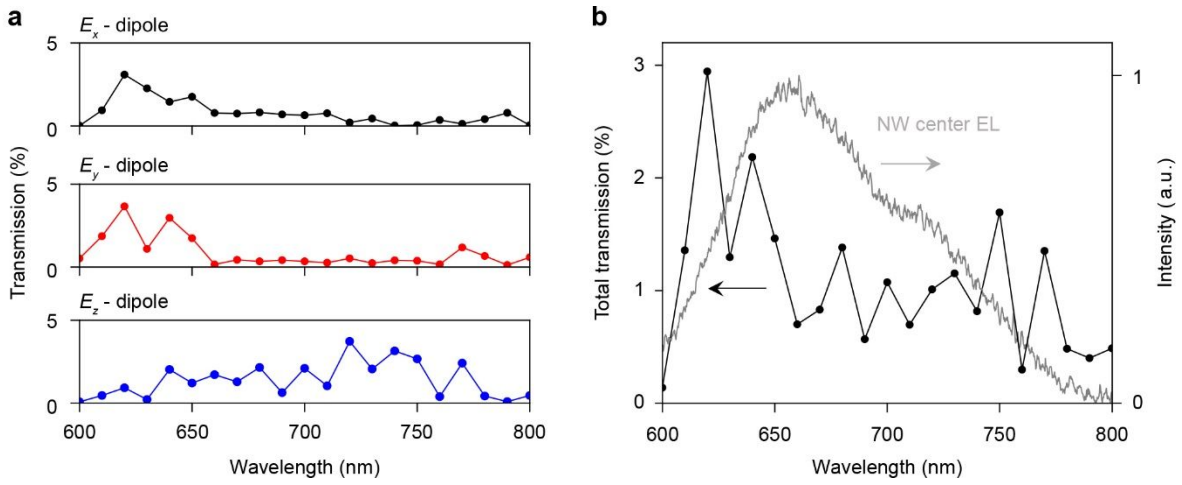

Figure S10. Calculated transmission results as a function of the dipole wavelength. (a) Calculated transmissions (i.e., P_{trans}/P_{dipole}) at a position 50 μm away from the NW. Top (black dots), middle (red dots), and bottom (blue dots) panels respectively show the transmission results for electric dipoles with E_x, E_y, and E_z polarizations. (b) Calculated total transmission, which sums the contributions from all of the dipoles (black dots)[12]: $T_{tot} = \sum_{i=x,y,z} P_{trans,i} / \sum_{i=x,y,z} P_{dipole,i}$. Note that we calculated the total transmission values under the condition of equal dipole powers for all wavelengths. To describe the experimental observations more accurately, the normalized spectral power of the NW (gray line) should be considered as a weighting factor for each dipole source. The weighted total transmission values were estimated and are plotted in Figure 4f of the Manuscript.

References

(1) Lee, J. M.; Choung, J. W.; Yi, J.; Lee, D. H.; Samal, M.; Yi, D. K.; Lee, C.-H.; Yi, G.-C.; Paik, U.; Rogers, J. A.; Park, W. I. Vertical Pillar-Superlattice Array and Graphene Hybrid Light Emitting Diodes. *Nano Lett.* **2010**, *10* (8), 2783–2788.

(2) Hanson, G. Dyadic Green's functions and guided surface waves for a surface conductivity model of graphene. *J. Appl. Phys.* **2008**, 103, 064302.

(3) Degli-Eredi, I.; Sipe, J. E.; Vermesulen N. TE-polarized graphene modes sustained by photonic crystal structures. *Opt. Lett.* **2015**, *40* (9), 2076-2079.

(4) Palik, E. D. *Handbook of Optical Constants of Solids*; Academic Press: San Diego, **1998**.

(5) Philipp, H. R. Optical Properties of Silicon Nitride. *J. Electrochem. Soc.* **1973**, 120 (2), 295–300.

(6) Cao, L.; White, J. S.; Park, J.-S.; Schuller, J. A.; Clemens, B. M.; Brongersma, M. L. Engineering light absorption in semiconductor nanowire devices. *Nat. Mater.* **2009**, *8* (8), 643–647.

(7) Kempa, T. J.; Cahoon, J. F.; Kim, S.-K.; Day, R. W.; Bell, D. C.; Park, H.-G.; Lieber, C. M. Coaxial multishell nanowires with high-quality electronic interfaces and tunable optical cavities for ultrathin photovoltaics. *Proc. Natl. Acad. Sci. U. S. A.* **2012**, *109* (5), 1407–1412.

(8) Duan, X.; Huang, Y.; Agarwal, R.; Lieber, C. M. Single-nanowire electrically driven lasers. *Nature* **2003**, *421* (6920), 241-245.

(9) Qian, F.; Gradečak, S.; Li, Y.; Wen, C.-Y.; Lieber, C. M. Core/Multishell Nanowire Heterostructures as Multicolor, High-Efficiency Light-Emitting Diodes. *Nano Lett.* **2005**, *5* (11), 2287–2291.

(10) No, Y.-S.; Choi, J.-H.; Ee, H.-S.; Hwang, M.-S.; Jeong, K.-Y.; Lee, E.-K.; Seo, M.-K.; Kwon, S.-H.; Park, H.-G. A Double-Strip Plasmonic Waveguide Coupled to an Electrically Driven Nanowire LED. *Nano Lett.* **2013**, *13* (2), 772–776.

(11) Fan, P.; Colombo, C.; Huang, K. C. Y.; Krogstrup, P.; Nygård, J.; Fontcuberta I Morral, A.; Brongersma, M. L. An Electrically-Driven GaAs Nanowire Surface Plasmon Source. *Nano Lett.* **2012**, *12* (9), 4943–4947.

(12) Henneghien, A.-L.; Gayral, B.; Désières, Y.; Gérard, J.-M. Simulation of waveguiding and emitting properties of semiconductor nanowires with hexagonal or circular sections. *J. Opt. Soc. Am. B*. **2009**, *26* (12), 2396-2403.